Theoretical and Experimental Investigation of Feedforward Signal Regeneration as a Means of Combating Multipath Propagation Effects in Pilot-Based SSB Mobile Radio Systems

JOSEPH P. McGEEHAN AND ANDREW J. BATEMAN

Abstract—**A technique is described, feedforward signal regeneration (FFSR), to combat the effects of multipath propagation on VHF and UHF pilot tone single sideband (SSB) mobile radio systems. Unlike feedforward automatic gain control (FFAGC), FFSR suppresses both the random amplitude and phase fluctuations in the received signal. Extensive laboratory and field tests have shown that the operation of SSB at UHF frequencies is a viable proposition for both speech and data communication.**

I. INTRODUCTION

AS A RESULT of the continually increasing demand for mobile communication systems world-wide, a considerable amount of research and development has been undertaken to establish spectrum efficient techniques and modes of information transmission. To this end, single sideband (SSB) has been the subject of much investigation by several research groups [1]-[3] in the U.S. and U.K. for use in future mobile radio links as a replacement for the FM and AM systems presently used. The imposition of rapid random amplitude and phase fluctuations on the received signal through the severe multipath propagation conditions, as well as the need for precise frequency reference in both the transmitter and receiver, has led to the inception of pilot-based SSB within a 5-kHz channel spacing. The transmission of a constant amplitude pilot tone, together with the desired information, provides an amplitude and phase reference which can be used for the automatic frequency control of the receiver local oscillators and for the pilot-based correction to counteract the unwanted modulation effects of multipath propagation. Unless suppressed, these random fluctuations can, at high-band VHF and UHF, cause considerable distortion of speech and data links. In the case of voice communications, the random amplitude fluctuations result in the speech sounding chopped or "gravelly," while the frequency fluctuations introduce "wow" and "flutter." These effects are particularly disturbing at UHF, where the random envelope fluctuations can occur at the syllabic rate. Clearly, if SSB is to be accepted as a quality carrier for the radiophone and private mobile radio services throughout the mobile frequency bands, techniques for reducing the multipath induced distortion must be established and fully investigated.

With respect to AM type systems, various techniques have been specifically developed or applied over the years to mitigate the effects of fading on channel quality. Feedback automatic gain control (FBAGC) has been employed to remove the slow log-normal variations in mean level of the received signal which arise through changing transmitter/receiver distances and gross variations in the environment surrounding the receiver. Now it has been shown elsewhere [4] that FBAGC of the exponential integrator type can only suppress fading adequately in the presence of audio information if it occurs at rates of less than a few Hertz. Furthermore, it has been shown that any attempt to suppress fully the more rapid fluctuations due to multipath propagation can lead to fading enhancement or, in the limit, loop instability, as a result of the inherent time delay in the AGC control loop of a pilot tone SSB receiver.

Diversity as a means of reducing multipath interference has been well documented [5], [6] and offers a partial solution to the problem by reducing the dynamic range of envelope fluctuations and improving the signal-to-noise (S/N) ratio. The implementation of such systems normally involves the use of multiple transmitter or multiple receiver aerial systems, together with special combining circuitry and, as such, can be prohibitively expensive.

Recent research by McGeehan and Burrows [7] into feedforward methods of gain correction, as distinct from feedback, has led to the development of feedforward AGC (FFAGC) which is capable of suppressing the fast envelope fading rates which can occur at high-band VHF and UHF. The system has been well documented and a detailed study of the performance limits undertaken. While providing adequate suppression of the random amplitude fluctuations, the technique has no effect in reducing the distortion due to the remaining phase fluctuations. In order for feedforward techniques to operate satisfactorily, unambiguous information describing the magnitude and phase of the multipath induced distortion must be extracted. The fading information has been shown [8] to be contained within the narrow bandwidth of twice Doppler frequency. Therefore, provided there is adequate separation between the pilot tone and its neighboring information components, it is possible to separate, by suitable filtering in the receiver, the spread pilot from the spread audio components without fear of spectrum overlap.

Manuscript received July 9, 1982; revised October 3, 1982. This work was supported in part by the U.K. Science and Engineering Research Council.

The authors are with the School of Electrical Engineering, University of Bath, Claverton Down, Bath BA2 7AY, Avon, England. Telephone 0225 61244 ext. 314 or school office.

0018-9545/83/0200-0106$01.00

The operation of removing only the amplitude fluctuations with FFAGC (or, for that matter, removing just the phase fluctuations by heterodyne phase stripping in certain diversity techniques) results in significant spreading of the pilot and speech components outside the range of twice Doppler as shown schematically in Fig. 1(a) and (b). This makes it difficult or even impossible to extract the pilot tone components for subsequent processing and complicates the removal of the pilot tone at the receiver output. Moreover, the subjective distortion arising from the remaining amplitude or phase fluctuations is enhanced and noticeably degrades the quality of the received output signal. However, by removing both the amplitude and phase fluctuations simultaneously, the pilot is regenerated as a single frequency component, thereby making the extraction and removal of the system reference tone in the later stages of receiver processing a relatively trivial affair. Such suppression of the imposed random modulation gives rise to the possibility of a high-quality low-distortion voice communications channel and an improved bit error rate performance in mobile data transmission systems. The generic name of such pilot-based correction systems has been designated by the authors as feedforward signal regeneration (FFSR).

In a recent paper by Leland and Sollenberger [9], a purely theoretical treatise of one such combined amplitude and phase correction system is given. The analysis assumes an idealized SSB channel, incorporating perfect system components, and concentrates upon the distortion introduced into such a system by frequency selective fading, cochannel pilot interference, and limits of the available gain correction (a mechanism similar to the threshold suggested by Burrows and McGeehan [10] for use with FFAGC). The analysis also encompassed the use of such a system with post-detection diversity as a means of improving the S/N performance.

The work presented in this paper is concerned with the engineering and analysis of FFSR for use in VHF and UHF mobile radio systems. Provided good correlation exists between the fading statistics of the pilot tone and that superimposed on the information signal, almost total suppression of the unwanted amplitude and phase fluctuations is shown to be obtainable. It is anticipated from the laboratory and field trials conducted, that with the possible addition of diversity to improve the S/N performance at low signal strengths, a high quality voice and data communications link at carrier frequencies up to 1 GHz can be established. In this context, besides removing the multipath induced distortion, FFSR will be shown to eliminate any frequency offset that may arise due to inaccuracies in the transmitter and receiver local oscillators. This allows the performance specifications of these oscillators and corresponding frequency control loops to be relaxed somewhat, thereby reducing system complexity and cost.

The FFSR processing is performed entirely at audio frequencies and can be readily integrated using current metal-oxide-semiconductor (MOS) technology in a dedicated form or, as pursued by the authors, in a software from using Intel 2920 analog microprocessors. The system described is compatible with all four types of pilot SSB currently under investigation: pilot carrier, tone-in-band, transparant tone-in-band

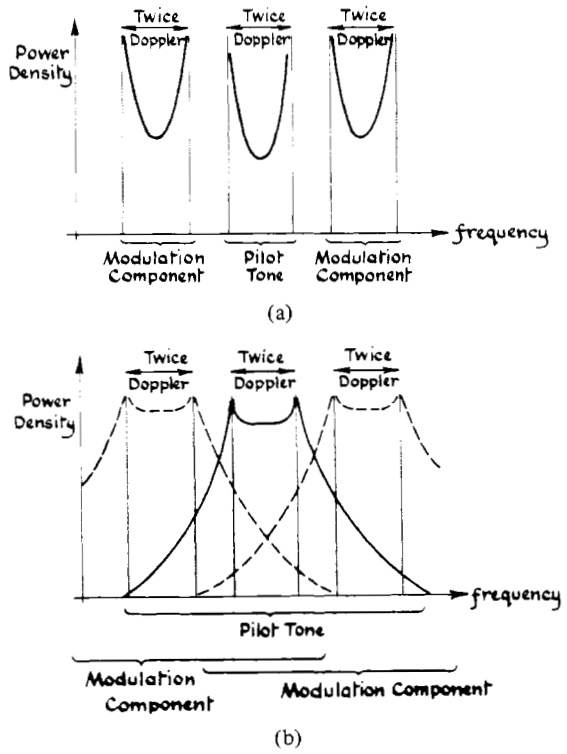

Fig. 1. (a) Received fading spectra. (b) Spread pilot and modulation spectra due to removal of either amplitude or phase fluctuations.

(TTIB) [11], and tone-above-band. However, for optimum performance in the fading environment at UHF and above, the use of transparent tone-in-band is shown to be preferable. Experimental results are presented from field tests conducted in and around the city of Bath with a 457 MHz TTIB SSB communications system.

II. PRINCIPLES OF FFSR OPERATION

To illustrate the salient features of FFSR operation, a mathematical description of the received fading signal $y_i(t)$ is utilized, where

$$y_i(t) = Ex(t)\cos(\omega_1 t + \omega_p t + y(t)) + Sx(t)\cos(\omega_1 t + \omega_s t + y(t)). \quad (1)$$

The random amplitude modulation is represented by $x(t)$ and the random phase modulation by $y(t)$. ω_p and ω_s are the angular frequencies of the pilot tone and audio signal components, respectively, with E and S the corresponding amplitudes. ω_1 represents an IF frequency of the receiver. The action of FFSR is to generate a control signal $\eta(t)$ at a second intermediate frequency ω_2 given by

$$\eta(t) = \frac{C}{x(t)}\cos(\omega_2 t + y(t)), \quad (2)$$

where C is a constant. By using $\eta(t)$ to mix down linearly the received signal $y_i(t)$, an output signal $y_0(t)$ is generated with both the unwanted random amplitude and phase varia-

tions, $x(t)$ and $y(t)$, removed:

$$y_0(t) = \frac{EC}{2}\cos((\omega_p t + (\omega_1 - \omega_2)t) + \frac{SC}{2}\cos((\omega_s t + (\omega_1 - \omega_2)t). \quad (3)$$

If the receiver is configured such that ω_1 equals ω_2 in the above expressions, the required signal is demodulated to baseband.

III. IMPLEMENTATION OF FFSR

In this section, two methods of implementing FFSR are described. The first technique operates at an intermediate frequency in the receiver and can be used with all types of pilot tone SSB currently being investigated. The second technique operates on the demodulated output of the receiver and can be regarded as an add-on convenience circuit. Its use is, however, restricted to tone-in-band, TTIB, and tone-above-band systems.

Method 1

A block diagram of the processing required is shown in Fig. 2. Let us assume that the signal at the input to the circuit, point A, is of the form:

$$g(t)_A = Ex(t)\cos(\omega_1 t + \omega_p t + \omega_e t + y(t)) + Sx(t)\cos(\omega_s t + \omega_1 t + \omega_e t + y(t)), \quad (4)$$

where ω_e represents the angular frequency error in the receiver IF frequency ω_1. After mixing and filtering to extract the fading pilot tone, the signal at point B is given by

$$g(t)_B = Ex(t)\cos((\omega_1 - \omega_2)t + \omega_p t + \omega_e t + y(t))|_{t\to t-\tau_a}. \quad (5)$$

Providing that the amplitude of the pilot envelope is above a predetermined threshold level, then the action of the processing within the block Z is to generate a control signal at point C of the form:

$$g(t)_C = \frac{M}{x(t)}\cos((\omega_1 - \omega_2)t + \omega_p t + \omega_e t + y(t))|_{t\to t-\tau_a-\tau_c}, \quad (6)$$

where M is a constant. If this control signal is now used to mix down linearly a delayed version of the input signal to the circuit, then the regenerated signal at point D is given by

$$g(t)_D = \frac{ME}{2}\cos\omega_2 t + \frac{MS}{2}\cos(\omega_s t + (\omega_2 - \omega_p)t)|_{t\to t-\tau_b-\tau_d}, \quad (7)$$

provided that the time delays in the upper and lower signal paths are matched, i.e., $\tau_b = \tau_a + \tau_c$. If $\omega_2 = \omega_p$, then the resulting output signal is correctly demodulated to baseband. For pilot carrier SSB systems, $\omega_2 = \omega_p = 0$ and the first mixer and oscillator in the control path can be removed.

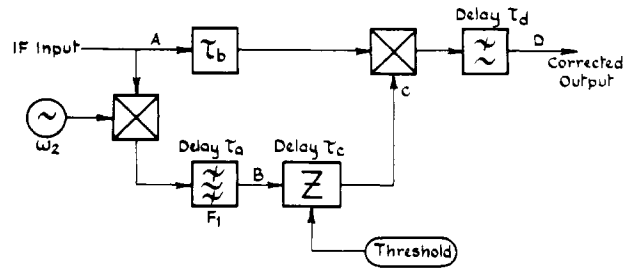

Fig. 2. FFSR processing—method 1.

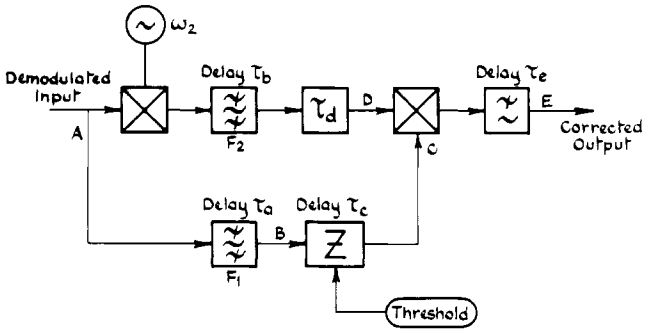

Fig. 3. FFSR processing—method 2.

Method 2

The operation of this particular form of FFSR circuitry is best understood by reference to Fig. 3. If the demodulated input at point A is expressed as

$$h(t)_A = Ex(t)\cos(\omega_p t + \omega_e t + y(t)) + Sx(t)\cos(\omega_s t + \omega_e t + y(t)), \quad (8)$$

then the fading pilot appearing at the output of the bandpass filter, point B, is

$$h(t)_B = Ex(t)\cos(\omega_p t + \omega_e t + y(t))|_{t\to t-\tau_a}. \quad (9)$$

Provided that the pilot envelope amplitude is above the threshold level, the control signal generated at point C is given by

$$h(t)_C = \frac{M}{x(t)}\cos(\omega_p t + \omega_e t + y(t))|_{t\to t-\tau_a-\tau_c}. \quad (10)$$

The frequency translated input signal at point D after filtering is

$$h(t)_D = Ex(t)\cos((\omega_p + \omega_2)t + \omega_e t + y(t)) + Sx(t)\cos(\omega_s t + \omega_2 t + \omega_e t + y(t))|_{t\to t-\tau_b-\tau_d} \quad (11)$$

which, after mixing with the control signal, $h(t)_C$, results in

a filtered output:

$$h(t)_E = \frac{EM}{2}\cos \omega_2 t + \frac{ES}{2}\cos\ (\omega_s t + (\omega_2 - \omega_p)t)\,|_{t\to t-\tau_b-\tau_d-\tau_e}, \tag{12}$$

provided the condition $(\tau_a + \tau_c) = (\tau_b + \tau_d)$ is satisfied. With $\omega_2 = \omega_p$, the output signal is demodulated to baseband.

It is noteworthy that both methods of implementation remove any frequency error ω_e from the input signal, thus compensating for any receiver mistuning arising from local oscillator drift in either the transmitter or receiver. While this property may not be a significant factor at HF and VHF, the problem of oscillator stability at UHF is paramount. Without the use of FFSR processing, the necessity of maintaining frequency errors to within a few Hertz, desirable for high quality speech communication systems, requires complicated and expensive synthesizer and frequency locking techniques.

Fading Pilot Tone Processing Module Z

The pilot tone processing denoted by the module Z in Figs. 2 and 3 can be performed in several ways depending on the type of implementation and application for which the FFSR system is intended. Fig. 4(a) and (b) shows two of the possible configurations which have been investigated experimentally.

The processing shown in Fig. 4(a) makes use of a full wave rectifier and low-pass filter to extract the pilot tone envelope. If the input signal at point a, representing the fading pilot, is assumed to be of the form

$$P(t)_a = x(t)\cos(\omega_p + y(t)), \tag{13}$$

then after full wave rectification the signal becomes

$$P(t)_b = k(x(t) + \text{components centered at } 2\omega_p, 4\omega_p, \cdots). \tag{14}$$

where k is a constant. Subsequent low-pass filtering extracts the envelope of the rectified signal giving

$$P(t)_c = k(x(t))\,|_{t\to t-\tau}. \tag{15}$$

At this point in the circuit, the threshold circuitry operates to give a signal at point d:

$$P(t)_d = k \max\{x(t), v_{\text{th}}\}\,|_{t\to t-\tau}, \tag{16}$$

where v_{th} represents the threshold level and max $\{\cdot,\cdot\}$ is defined as the larger of the two arguments on an instantaneous basis. The resulting control signal is thus

$$P(t)_e = \left.\frac{x(t)\cos(\omega_p t + y(t))}{k^2 \max\{x^2(t), v_{\text{th}}{}^2\}}\right|_{t\to t-\tau} \tag{17}$$

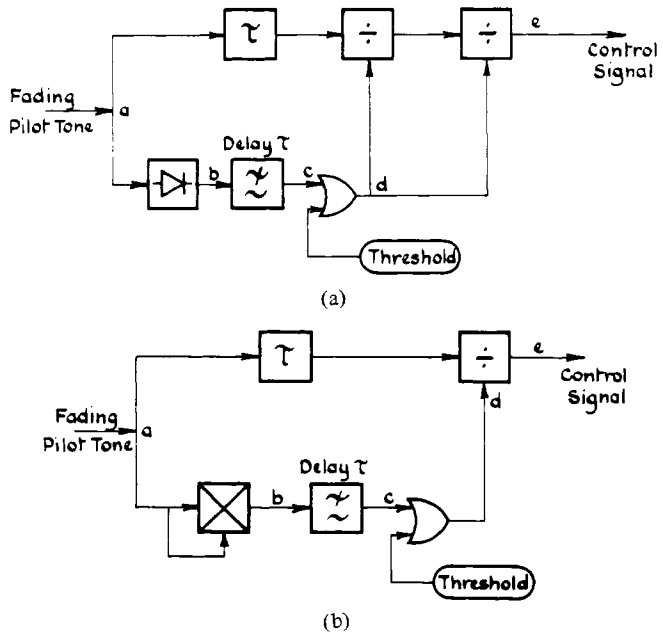

Fig. 4. (a) Implementation of pilot tone processing Z. (b) Alternative implementation of Z.

which for $x(t) > v_{\text{th}}$ becomes

$$P(t)_e = \frac{K'}{x(t)}\cos(\omega_p t + y(t))\,|_{t\to t-\tau}. \tag{18}$$

The second method of implementation for the module Z as shown in Fig. 4(b), uses a squaring detector for envelope extraction. If the configuration is subject to the same fading pilot input signal described by equation (13), the output of the mixer at point b is then

$$P(t)_b = k(x^2(t) + x^2(t)\cos 2(\omega_p t + y(t)). \tag{19}$$

After passing through the low-pass filter to remove the 2ω term,

$$P(t)_c = kx^2(t)\,|_{t\to t-\tau}, \tag{20}$$

which means that the signal at the output of the threshold is

$$P(t)_d = k \max\{x^2(t), v_{\text{th}}\}\,|_{t\to t-\tau}, \tag{21}$$

resulting in a control signal

$$P(t)_e = \left.\frac{k'x(t)\cos(\omega_p t + y(t))}{\max\{x^2(t), v_{\text{th}}\}}\right|_{t\to t-\tau}. \tag{22}$$

For $x^2(t)$ greater than the threshold level v_{th}, the control signal becomes

$$P(t)_e = \frac{k'}{x(t)}\cos(\omega_p t + y(t))\,|_{t\to t-\tau}. \tag{23}$$

Both of the Z modules described generate the same control

signal $P(t)_e$. However, due to the squaring action of the envelope processing in Fig. 4(b), the resulting dynamic range requirements, measured in decibels, for the subsequent circuitry must be doubled in comparison with that used in the alternate processing arrangement of Fig. 4(a). The justification for using "squarer-type" envelope detection lies in the restriction of the generated harmonics to within twice the pilot tone frequency and, as will be shown later, the restriction of the harmonics of the envelope term $x^2(t)$ to within twice Doppler frequency. The frequency spectra for the envelope and (envelope)^2 of a fading tone recorded in the field are shown in Fig. 12. In contrast, the full wave rectification process generates infinite even order harmonics of the pilot tone with the phase error $y(t)$ superimposed and results in the significant harmonic content of the envelope $x(t)$ extending to several times the Doppler frequency. These effects make it difficult or impossible to separate the pilot envelope completely from the pilot tone related harmonics.

IV. PERFORMANCE SENSITIVITY FOR A NONIDEAL FFSR SYSTEM

In this section, the performance of an FFSR system is analyzed when the system contains nonideal circuit elements and when the system itself is contained within a nonidealized SSB receiver.

In the urban mobile radio environment, a line-of-sight path between transmitter and receiver seldom exists, and the received fading pilot tone has its spectrum smeared to the familiar U shape, as shown in Fig. 1(a), by multipath propagation effects. The components of greatest magnitude occur at plus and minus Doppler frequency. For this reason and in an attempt to use a worst-case test signal for sensitivity analysis, the pilot tone when subject to multipath fading is assumed to be operated upon by M where

$$M(f(t)) = f(t)\,|_{\omega\to(\omega-\omega_d)} + R(f(t))\,|_{\omega\to(\omega+\omega_d)}. \tag{24}$$

If the received pilot in the absence of fading is given by

$$P(t) = E\cos\omega_p t, \tag{25}$$

then under the influence of the operator M, the pilot is modified to

$$M(P(t)) = E\cos(\omega_p t - \omega_d t) + RE(\omega_p t + \omega_d t). \tag{26}$$

For convenience in the ensuing analysis, we reformulate this equation as an amplitude and phase modulated carrier as follows:

$$M(P(t)) = E(1 + R^2 + 2R\cos 2\omega_d t)^{1/2} \cdot \cos\left\{\omega_p t - \tan^{-1}\left(\frac{\sin\omega_d t - R\sin\omega_d t}{\cos\omega_d t + R\cos\omega_d t}\right)\right\}. \tag{27}$$

The envelope term which is given by

$$x(t) = E(1 + R^2 + 2R\cos 2\omega_d t)^{1/2} \tag{28}$$

consists of an infinite number of harmonics occurring at multiples of twice Doppler frequency. However, by squaring the envelope function to give

$$x^2(t) = E^2(1 + R^2 + 2R\cos 2\omega_d t), \tag{29}$$

the resulting frequency spectrum is contained within twice Doppler as required. It is easily shown that, for a signal containing an infinite number of tones within the range twice Doppler, the frequency components of the envelope squared are also contained within twice Doppler frequency.

By applying $M(P(t))$ as the input signal to the FFSR processing shown in Figs. 2 and 3, it is possible to analyze the effects of nonconstant passband gain and deviations from linear phase for the bandpass filters F_1 and F_2 and time delay mismatch between the upper and lower processing paths as follows.

Let us assume the filter characteristics of F_1 and F_2 are as shown in Fig. 5(a) and (b). With reference to Fig. 3, the pilot tone after filtering by F_1 is given by

$$M(P(t)) = EA_1\cos(\omega_p - \omega_d)(t - \tau_a - \tau_{a1}) + ERA_2\cos(\omega_p + \omega_d)(t - \tau_a - \tau_{a2}), \tag{30}$$

which can be rewritten as

$$M(P(t)) = s(t)\cos(\omega_p t - u(t)), \tag{31}$$

where $s(t)$ and $u(t)$ are given by

$$s(t) = EA_1(1 + R^2A^2 + 2RA\cos\{2\omega_d t + (\omega_p - \omega_d)(\tau_a + \tau_{a1}) - (\omega_p + \omega_d)(\tau_a + \tau_{a2})\})^{1/2} \tag{32}$$

$$u(t) = \tan^{-1}\left\{\frac{\sin(\omega_d t + (\omega_p - \omega_d)(\tau_a + \tau_{a1})) - RA\sin(\omega_d t - (\omega_p + \omega_d)(\tau_a + \tau_{a2}))}{\cos(\omega_d t + (\omega_p - \omega_d)(\tau_a + \tau_{a1})) + RA\cos(\omega_d t - (\omega_p + \omega_d)(\tau_a + \tau_{a2}))}\right\} \tag{33}$$

with $A = A_2/A_1$.

After being processed by the module Z, the resulting delayed control signal at point C of Fig. 3 for $s(t)$ above threshold level is

$$M(P(t))_C = \frac{1}{s(t)}\cos(\omega_p t - u(t))\,|_{t\to t-\tau_c}. \tag{34}$$

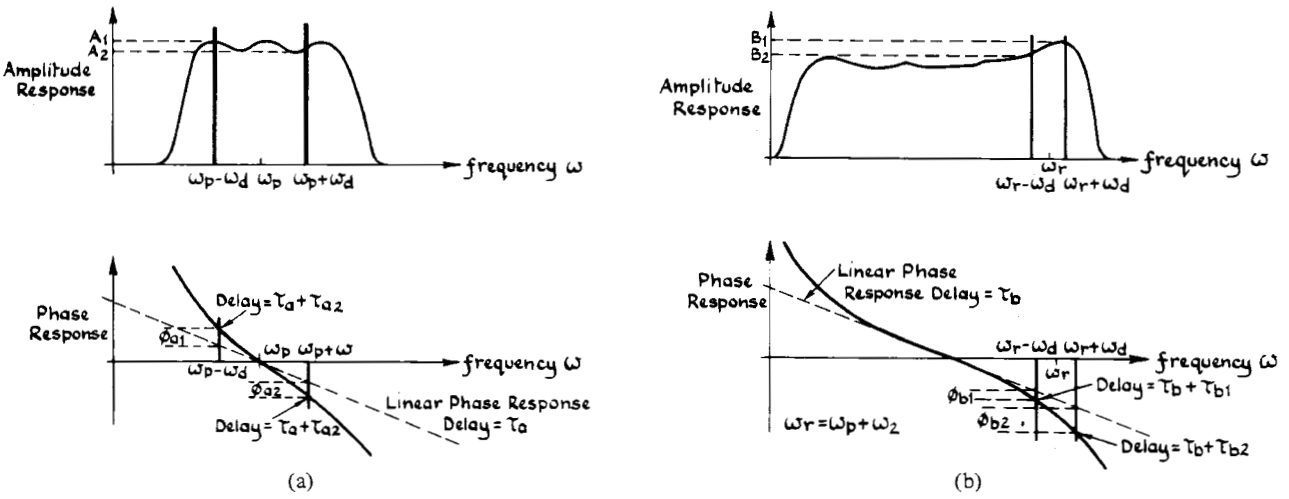

Fig. 5. Characteristics of filters. (a) f_1. (b) f_2.

A similar treatment of the translated signal at point D yields

$$M(P(t))_D = e(t) \cos (\omega_r t - q(t))\,|_{t \to t-\tau_d}, \tag{35}$$

where $e(t)$ and $q(t)$ represent

$$e(t) = EB_1(1 + R^2B^2 + 2RB \cos \{2\omega_d t + (\omega_r - \omega_d)(\tau_b + \tau_{b1}) - (\omega_r + \omega_d)(\tau_b + \tau_{b2})\})^{1/2} \tag{36}$$

$$q(t) = \tan^{-1} \left\{ \frac{\sin (\omega_d t + (\omega_r - \omega_d)(\tau_b + \tau_{b1})) - RB \sin (\omega_d t - (\omega_r + \omega_d)(\tau_b + \tau_{b2}))}{\cos (\omega_d t + (\omega_r - \omega_d)(\tau_b + \tau_{b1})) + RB \cos (\omega_d t - (\omega_r + \omega_d)(\tau_b + \tau_{b2}))} \right\} \tag{37}$$

with $B = B_2/B_1$ and $\omega_r = \omega_p + \omega_2$.

If we assume that the time delays τ_c and τ_d can be equalized, then the regenerated signal obtained by linearly mixing $M(P(t))_C$ and $M(P(t))_D$ and filtering out the sum term, is

$$M(P(t))_E = \frac{e(t)}{s(t)} \cos (\omega_2 t + u(t) - q(t))\,|_{t \to t-\tau}, \tag{38}$$

where $\tau = \tau_c + \tau_e = \tau_d + \tau_e$.

The regenerated envelope $r(t)$ is consequently

$$r(t) = \frac{e(t)}{s(t)} = \frac{A_1}{B_1} \frac{(1 + R^2A^2 + 2RA \cos \{(2\omega_d t + (\omega_p - \omega_d)(\tau_a + \tau_{a1}) - (\omega_p + \omega_d)(\tau_a + \tau_{a2})\})^{1/2}}{(1 + R^2B^2 + 2RB \cos \{(2\omega_d t + (\omega_r - \omega_d)(\tau_b + \tau_{b1}) - (\omega_r + \omega_d)(\tau_b + \tau_{b2})\})^{1/2}} \tag{39}$$

and the residual phase error $v(t)$ given by

$$\begin{aligned} v(t) &= u(t) - q(t) \\ &= \tan^{-1} \left\{ \frac{\sin (\omega_d t + (\omega_p - \omega_d)(\tau_a + \tau_{a1})) - RA \sin (\omega_d t - (\omega_p + \omega_d)(\tau_a + \tau_{a2}))}{\cos (\omega_d t + (\omega_p - \omega_d)(\tau_a + \tau_{a1})) + RA \cos (\omega_d t - (\omega_p + \omega_d)(\tau_a + \tau_{a2}))} \right\} \\ &\quad - \tan^{-1} \left\{ \frac{\sin (\omega_d t + (\omega_p - \omega_d)(\tau_b + \tau_{b1}) - RB \sin (\omega_d t - (\omega_p + \omega_d)(\tau_b + \tau_{b1}))}{\cos (\omega_d t + (\omega_p - \omega_d)(\tau_b + \tau_{b1}) + RB \cos (\omega_d t - (\omega_r + \omega_d)(\tau_b + \tau_{b1}))} \right\}. \end{aligned} \tag{40}$$

A. Residual Amplitude and Phase Modulation

Let us now compare the regenerated pilot tone with the fading input pilot tone and for ease of comparison, the amplitude and phase terms will be considered separately.

Defining modulation depth J as

$$J = \frac{\text{maximum pilot amplitude}}{\text{minimum pilot amplitude}} \tag{41}$$

or, alternatively,

$$J \text{ (dB's)} = 20 \log_{10} (J), \tag{42}$$

then the modulation depth of the input signal $M(P(t))$ from (27) is given by

$$J_i = \frac{(1 + R^2 + 2R)^{1/2}}{(1 + R^2 - 2R)^{1/2}} = \frac{1 + R}{1 - R}, \tag{43}$$

and the modulation depth of the regenerated output signal

$M(P(t))_E$ is shown in Appendix I to be

$$J = \frac{1 - GH\cos(\alpha-\beta) + \sqrt{G^2H^2\cos^2(\alpha-\beta) - G^2H^2 + G^2 + H^2 - 2GH\cos(\alpha-\beta)}}{1 - GH\cos(\alpha-\beta) - \sqrt{G^2H^2\cos^2(\alpha-\beta) - G^2H^2 + G^2 + H^2 - 2GH\cos(\alpha-\beta)}} \tag{44}$$

when

$$G = \frac{2RA}{1+R^2A^2} \tag{45}$$

$$H = \frac{2RB}{1+R^2B^2} \tag{46}$$

$$\alpha = (\omega_p - \omega_d)(\tau_a + \tau_{a1}) - (\omega_p + \omega_d)(\tau_a + \tau_{a2}) \tag{47}$$

$$\beta = (\omega_r - \omega_d)(\tau_b + \tau_{b1}) - (\omega_r + \omega_d)(\tau_b + \tau_{b2}). \tag{48}$$

Regarding the residual phase modulation $v(t)$, it is more convenient and perhaps meaningful for analysis purposes to express it as an instantaneous frequency deviation $d(t)$ from the required single frequency component, ω_r. For the input signal $M(P(t))$, it is shown in Appendix II that the input deviation is given by

$$d_i(t) = \frac{(1-R^2)\omega_d}{1+R^2+2R\cos 2\omega_d t} \tag{49}$$

with the maximum value

$$d_i(t)_{\max} = \frac{1+R}{1-R}\omega_d. \tag{50}$$

The corresponding instantaneous frequency deviation of the corrected output, $d_0(t)$, is given by

$$d_0(t) = \frac{(1-R^2B^2)\omega_d}{1+R^2B^2+2RB\cos(2\omega_d t+\beta)} \cdot \frac{(1-R^2A^2)\omega_d}{1+R^2A^2+2RA\cos(2\omega_d t+\alpha)}. \tag{51}$$

No readily determinable analytic solution exists for the maximum value of $d_0(t)$, although the magnitude for specific values of A, B, α, and β can be found by computer simulation. This has been performed for the specific and simplified case of $B = 1$ and $\tau_{b1} = \tau_{b2} = 0$, corresponding to the processing shown in Fig. 2 with the filter F_2 replaced by a perfect delay element such that $\tau_a = \tau_b$. The instantaneous frequency deviation for this case is given by

$$d_0(t) = \frac{(1-R^2)\omega_d}{1+R^2+2R\cos 2\omega_d t} - \frac{(1-R^2A^2)\omega_d}{1+R^2A^2+2RA\cos(2\omega_d t+\theta)}\Big|_{t\to t-\tau_a} \tag{52}$$

where

$$\theta = (\omega_p - \omega_d)\tau_{a1} - (\omega_p + \omega_d)\tau_{a2} \tag{53}$$

corresponding to the total phase error, introduced by the filter F_1, from the linear phase response at the frequencies $(\omega_p - \omega_d)$ and $(\omega_p + \omega_d)$. The results obtained from the simulation for the maximum frequency deviation of the regenerated output with respect to the filter passband ripple A and the phase error θ are depicted in Fig. 6 at modulation depths of 10, 20, and 30 dB. The results are normalized by the maximum instantaneous frequency deviation of the input, as given by (50). A similar set of curves, shown in Fig. 7, for the residual modulation depth can be obtained from (44), by making the following substitutions:

$$H = \frac{2R}{1+R^2} \tag{54}$$

$$\alpha = \theta \tag{55}$$

$$\beta = 0. \tag{56}$$

If, for example, it is required that a fading input signal, having a 30-dB fade depth, be regenerated to a single tone with maximum amplitude modulation of 3 dB and instantaneous frequency duration reduced to, say, a third of that at the system input, then appropriate constraints on the characteristics of the pilot filter F_1 are that the phase deviation from a linear phase response be less than 2°, i.e., $\theta = 0.035$ radians, and that the passband ripple be less than 0.15 dB, i.e., $A = 1.0174$.

B. Pilot Filter Stopband Requirements

The filter stopband requirements can be specified in terms of the permissible output envelope modulation and residual instantaneous frequency deviation, when subject to an interfering speech or data component (lying within the filter stopband) of the form

$$x_i(t) = I\cos(\omega_i t + \psi), \tag{57}$$

where ω_i is the frequency of the interfering signal and I is the peak amplitude of the interference at the output of the filter. The effects of such an interference on the frequency deviation of the regenerated signal are complex and not considered further here. The contribution to the residual amplitude modulation is, however, more readily determined.

Assume that the envelope of the pilot signal is given by

$$x(t) = E(1+R^2+2R\cos 2\omega_d t)^{1/2} \tag{58}$$

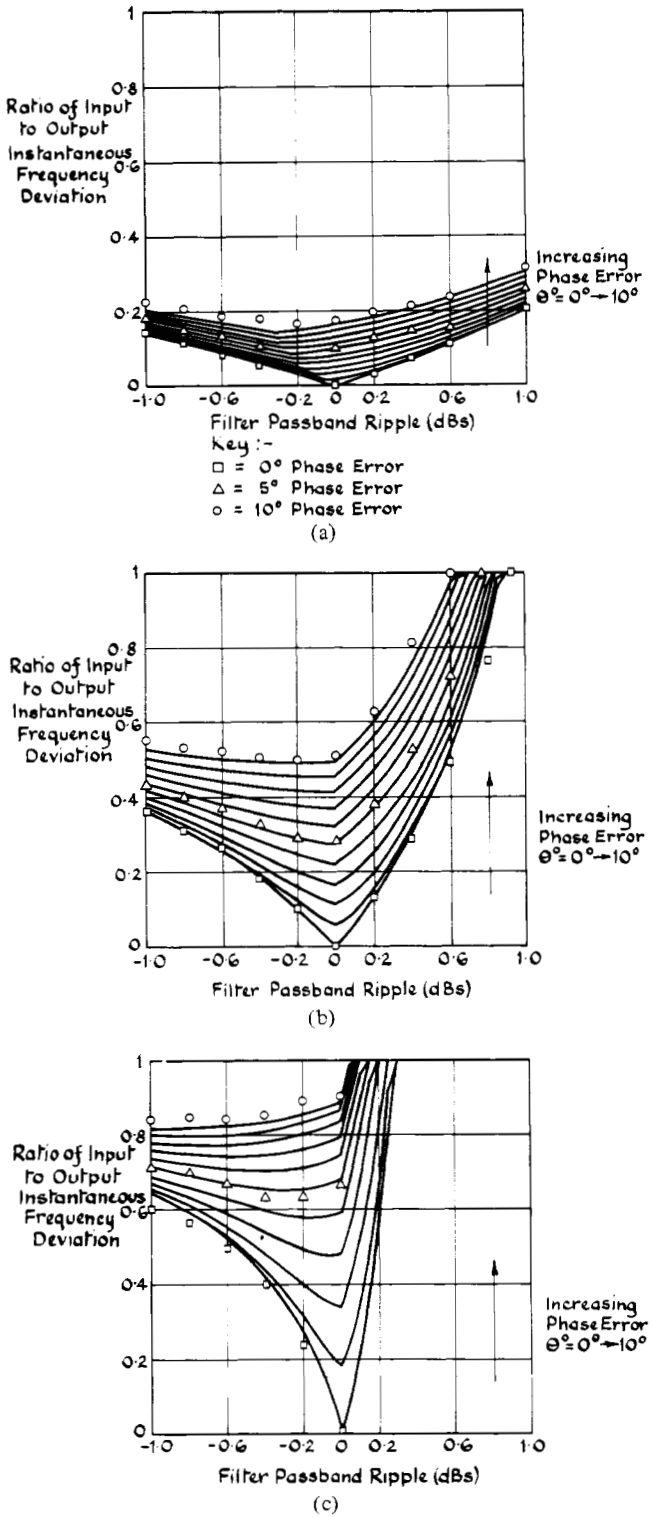

Fig. 6. Input fade depth. (a) 10 dB. (b) 20 dB. (c) 30 dB.

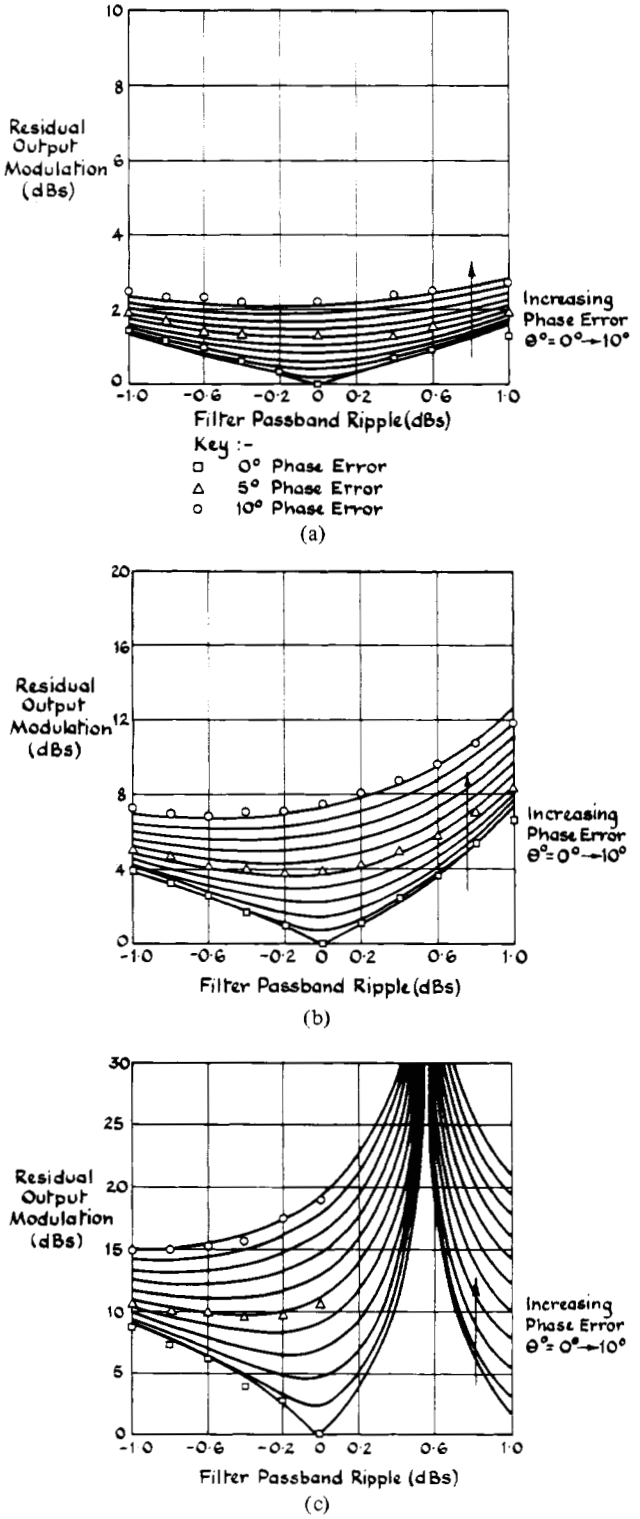

Fig. 7. Input fade depth. (a) 10 dB. (b) 20 dB. (c) 30 dB.

such that the maximum and minimum values are

$$x(t)_{\max} = E(1+R)$$
$$x(t)_{\min} = E(1-R). \tag{59}$$

The effect of the interferer is to modify these values to give

$$x_i(t)_{\max} = E(|1+RA|)$$
$$x_i(t)_{\min} = E(|1-RA|), \tag{60}$$

where A is given by

$$A = 1 + \frac{I}{ER}. \tag{61}$$

The resulting envelope modulation of the FFSR output has a maximum modulation depth J_0, where

$$J_0 = \frac{1-R}{1-RA}\,\frac{1+RA}{1+R}. \tag{62}$$

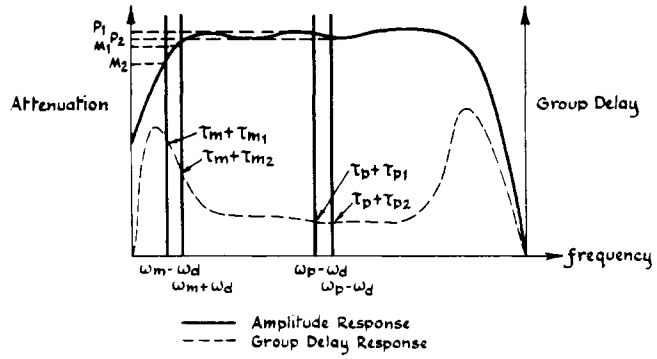

Fig. 8. Theoretical IF filter characteristic.

From (61) and (62), the value of A, and hence the maximum pilot-to-interference level E/I, permissible for a given modulation depth, can be calculated. Alternatively, A can be obtained directly from the zero phase error curves shown in Figs. 7(a)-(c). For example, to ensure a residual modulation depth of less than 3 dB for a 30-dB input fade depth, the above expression gives a pilot-to-interferer ratio $E/I = 0.0175$, corresponding to a required stopband attenuation of greater than 35 dB with respect to the pilot tone level.

C. Decorrelation Resulting from Receiver Prefiltering

So far, our theoretical analysis has made no provision for imperfections in the receiver processing. The major source of error to FFSR operation is decorrelation between the random modulation impressed upon the pilot reference and that impressed on the transmitted speech or data signal; it is almost entirely attributable to the IF crystal filter. A typical SSB filter characteristic is shown in Fig. 8. By making the following substitutions, (44)-(46) and (51) can be used to calculate the depth of residual modulation and instantaneous frequency error of the regenerated output arising from the imperfections in the IF filter response:

$$A = P_2/P_1 \tag{63}$$

$$B = M_2/M_1 \tag{64}$$

$$\alpha = (\omega_p - \omega_d)(\tau_p + \tau_{p1}) - (\omega_p + \omega_d)(\tau_p + \tau_{p2}) \tag{65}$$

$$\beta = (\omega_m - \omega_d)(\tau_m + \tau_{m1}) - (\omega_m + \omega_d)(\tau_m + \tau_{m2}). \tag{66}$$

If it is assumed that the differential group delay across the frequency band of twice Doppler is insignificant compared with the differential delay between pilot and modulation component $m(t)$ and, furthermore, that the amplitude response at the pilot frequency is flat, then the expressions can be simplified to

$$A = 1 \tag{67a}$$

$$B = M_2/M_1 \tag{67b}$$

$$\alpha = 0 \tag{67c}$$

$$\beta = -2\omega_d(\tau_m - \tau_p). \tag{67d}$$

Using the expressions, the FFSR output envelope modulation depth and maximum instantaneous frequency deviation can be obtained directly from the graphs in Figs. 6 and 7, where B represents the filter passband ripple and β the effective phase error from a perfect linear phase response.

Clearly, the decorrelation effect will be most pronounced for those modulation components positioned at the extremities of the IF filter passband. If the pilot reference is positioned close to the filter edge, as is the case in pilot carrier and tone-above-band SSB systems, the decorrelation, and therefore the residual modulation, of the regenerated modulation components over the central portion of the passband, will be particularly enhanced.

Consider the case of a tone-above-band system designed to operate in a 5-kHz channel spacing with a typical IF crystal filter characteristic as shown in Fig. 9. Assuming an audio bandwidth of 300 Hz-3 kHz and a pilot positioned at 3.2 kHz, the corresponding group delay error between the pilot and a modulation component centred in the audio band at 2 kHz is approximately 250 μs. Moreover, for a Doppler frequency shift of 50 Hz, corresponding to a vehicle speed of 112 km/h at 457 MHz, the measured filter roll-off at the pilot frequency could lead to an actual passband ripple of about 0.5 dB. In consequence, the output modulation and frequency deviation for a modest 20-dB input fade depth can only be reduced to 8 dB and by a factor of 0.2, respectively. The decorrelation due to prefiltering can be compensated for by the incorporation of suitable amplitude and phase equalization filters prior to the FFSR circuitry. Furthermore, the degree of decorrelation can be reduced before the application of such equilization techniques by using a wider IF filter and frequency offset schemes [12]. However, by placing the pilot in the central region of the band, the pilot and modulation components will have excellent correlation over the frequency range from 500 Hz to 3 kHz.

V. FFSR CIRCUIT IMPLEMENTATION

For SSB to be a viable commercial proposition, the majority of the signal processing is performed at audio frequencies, and the emphasis in our circuit design has been toward an integrated system, involving in these early stages of development an analog microprocessor.

Clearly, complete system integration may, through economic constraints, ultimately lie in dedicated hardware circuit integration as opposed to the more flexible software implementation. A schematic diagram of the actual FFSR system implemented is shown in Fig. 10.

Due to the stringent requirements placed on the pilot tone extraction filter F_1, in terms of phase linearity, passband ripple, and stopband attenuation, a dedicated integrated circuit incorporating a 64-tap nonrecursive bandpass filter has been utilized. The subsequent pilot tone processing and final demodulation are incorporated within the microprocessor, an Intel 2920-16. The envelope detection is of the squarer lowpass filter type described previously and is designed to minimize aliasing resulting from pilot tone harmonics. The envelope filter is also a nonrecursive transversal configuration to achieve linear phase response. Time delay τ_2 is introduced to equalize the delay in the filter F_2. The sum frequency term

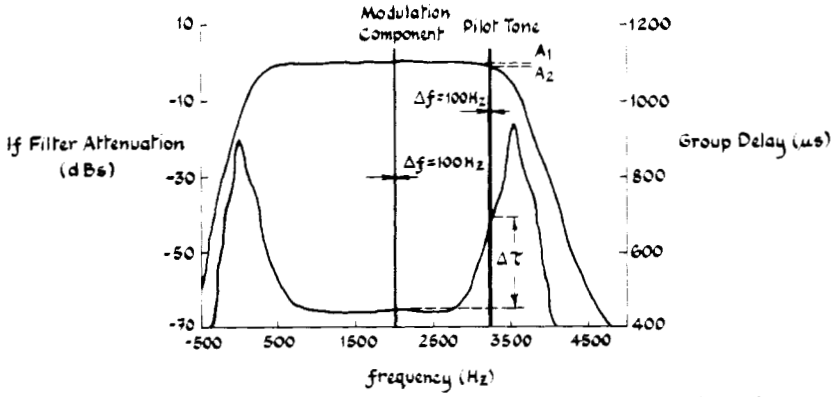

Fig. 9. Typical IF crystal filter characteristic for 5 kHz channel spacing.

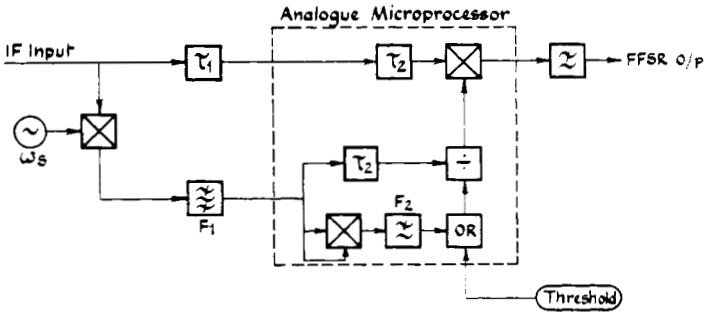

Fig. 10. Signal processing for FFSR.

generated in the final demodulation is removed by the external low-pass filter to give the regenerated output at baseband.

The requirement for a variable threshold in the envelope processing path has been outlined in an earlier paper by McGeehan and Burrows [7] when dealing with random gain modulation in FFAGC systems. With no imposed threshold, noise bursts occur at the receiver output as the pilot fades into the noise flow at low signal strengths. By limiting the gain of the FFSR processing with a variable threshold, the effect of random modulation and noise bursts are greatly reduced. An additional technique for improving the low signal strength performance of FFSR is the deployment of syllabic amplitude companding [13], [14]. This can reduce interword noise bursts and improves the apparent S/N ratio during syllables. The merit of dual threshold and companding systems are discussed further in the following section.

VI. EXPERIMENTAL RESULTS

Using the prototype FFSR circuit described thus far, extensive laboratory tests were performed using a two-tone test signal and a Rayleigh fading simulator [15]. Furthermore, field trials were undertaken in and around the City of Bath with the FFSR processing incorporated in a TTIB SSB mobile communications system operating at 457 MHz. Limited trials with an identical SSB processing system have also been conducted at 942 MHz.

In order to verify the theoretical performance of FFSR outlined in Section IV, measurements of residual amplitude and frequency modulation were taken for various simulated values of amplitude ripple and phase error in the pilot tone bandpass filter. A wide-band phase-locked loop was used to track the phase deviations of the corrected output, the VCO control voltage providing a direct measure of the instantaneous frequency deviation. The experimentally determined points are plotted together with the theoretical curves in Figs. 6 and 7, and excellent agreement between theory and practice is observed over the operating range of the prototype FFSR circuit, typically 35 dB and 100 Hz Doppler.

Field trials have shown that the use of FFSR in the multipath environment can give a marked improvement in the quality and intelligibility of voice communications. At the higher signal strengths (>30 μV EMF), the distortion occurring as a result of the residual random amplitude and phase fluctuations is negligible, while at low signal strengths (<10 μV EMF), the use of a threshold to reduce the noise bursts and amplitude companding to improve the subjective S/N performance further give rise to a much increased intelligibility for the SSB system. With the threshold disengaged, the subjective performance of the 942 MHz SSB system under low signal strengths is not dissimilar to that described by Arrendondo and Smith [16] for an 850-MHz FM mobile radio system under low signal strength conditions. By engaging the threshold, noise bursts occurring with the SSB system can be greatly reduced with subsequent improvement in subjective performance.

Preliminary data tests using 1200-baud FSK and DPSK have shown that the ability of FFSR to remove the random amplitude and phase fluctuations will substantially reduce the error probability in SSB systems, particularly as the Doppler frequency shift increases with the use of SSB at 900 MHz and above. These measurements together with the relevant theory will be the subject of a further publication. The outcome of an interesting series of benchmark tests are depicted in Figs. 11(a)-(l). Figs. 11(a), (b), and (c) show the time waveform and corresponding instantaneous frequency deviation and frequency spectra of a pilot tone recorded in the field using a 457 MHz SSB system. The average Doppler frequency over the run duration is 25 Hz. The remaining waveforms in Fig. 11 illustrate the effect of processing the fading pilot tone waveform in Fig. 11(a) with feedforward AGC, feedforward AFC, and FFSR circuits. Figs. 11(d)-(f) and (g)-(i) clearly show that while FFAGC and FFAFC compensate for amplitude and phase fluctuations, respectively, the corresponding phase and amplitude waveforms are, if anything, slightly worsened as a

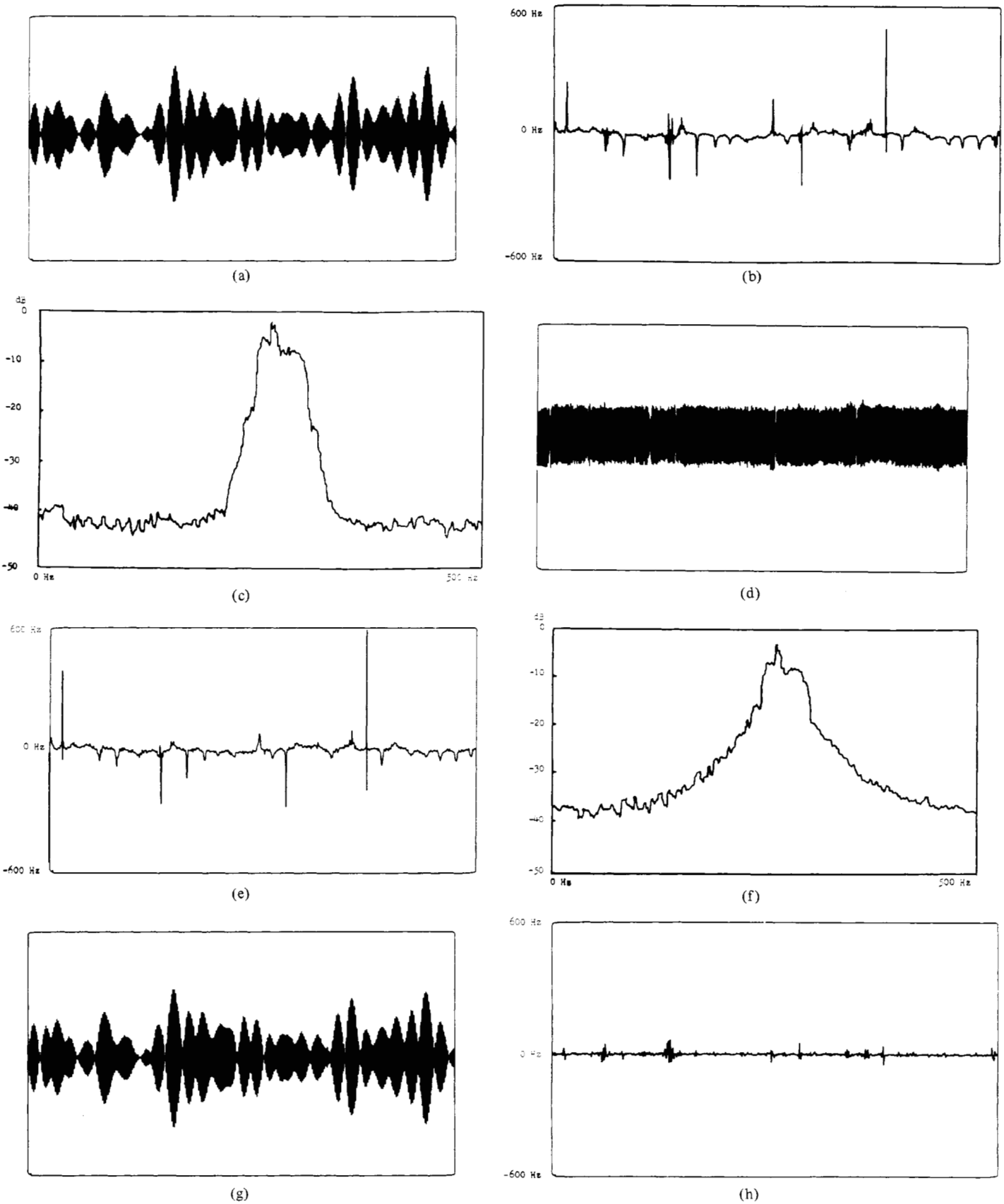

Fig. 11. (a) Envelope variation (FFSR circuit input). (b) Instantaneous frequency deviation (FFSR circuit input). (c) Power density spectrum (FFSR circuit input). (d) Envelope variations (FFAGC output). (e) Instantaneous frequency deviation (FFAGC output). (f) Power density spectrum (FFAGC output). (g) Envelope variation (FFAFC output). (h) Instantaneous frequency deviation (FFAFC output). (i) Power density spectrum (FFAFC output). (j) Envelope variation (FFSR output). (k) Instantaneous frequency deviation (FFSR output). (1) Power density specturm (FFSR output).

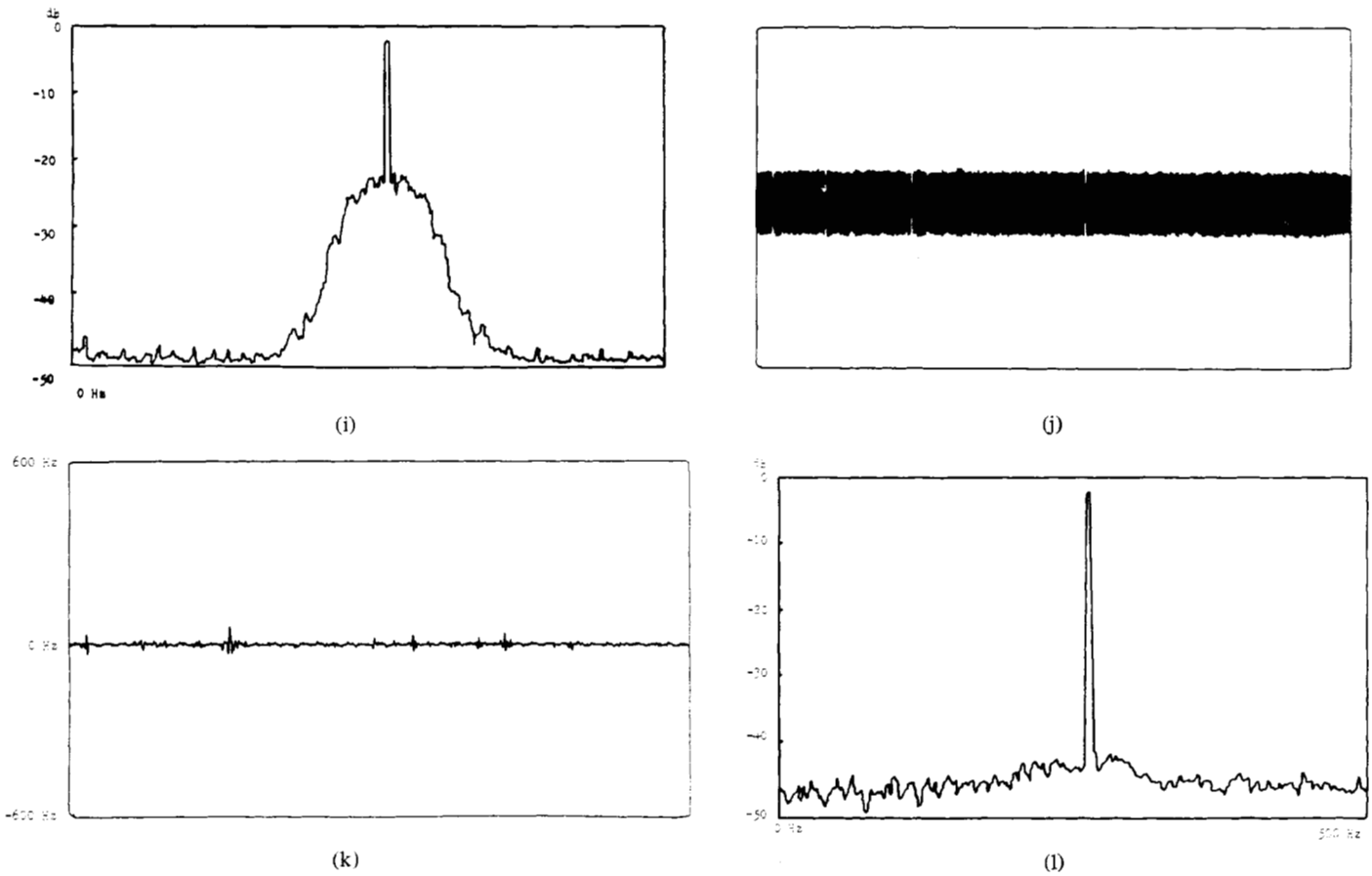

Fig. 11. (*Continued*)

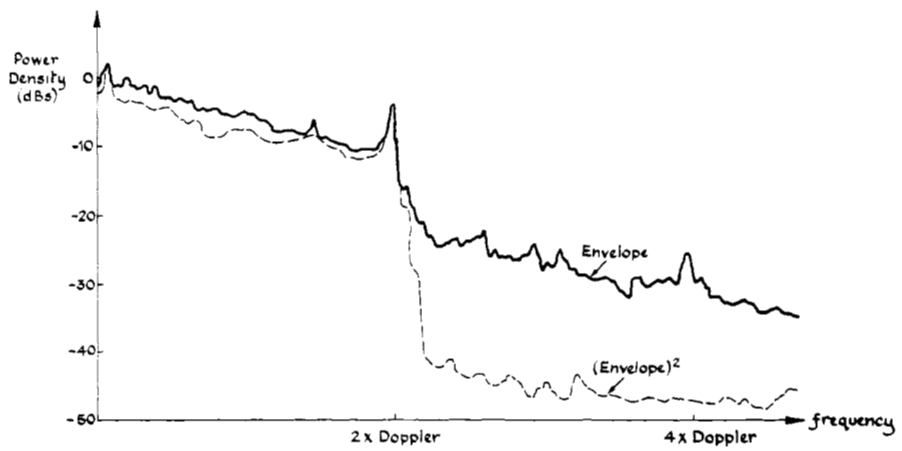

Fig. 12. Power density spectra of fading pilot tone envelope and (envelope)^2.

result of spectra spreading. The spreading effect of FFAGC and FFAFC may be observed by comparing Figs. 11(f) and (i) with Fig. 11(c). The output frequency spectra of the FFAFC circuit, shown in Fig. 11(i), is particularly revealing; in removing the random FM from the received signal, the pilot tone has been left with two "sidebands" from the remaining random amplitude fluctuations. If the waveform sets described hitherto are now compared with the corresponding waveforms obtained with the FFSR system in circuit, the potential of utilizing UHF pilot tone SSB communications is immediately realized.

VII. CONCLUSION

The FFSR system described has been shown to be capable of successfully combating the rapid amplitude and phase fluctuations which occur as a result of the severe multipath propagation in the mobile radio environment. Furthermore, it can eliminate frequency errors which arise through drift in the transmitter and receiver local oscillators, thereby relaxing somewhat the specification for low phase noise, high stability frequency sources and reducing the complexity of frequency control system. Taken together, the potential advantage of using pilot tone SSB systems up to 1 GHz can now be considered.

Laboratory measurements and field trails have demonstrated the system's ability to improve the subjective performance of speech communications dramatically, and preliminary studies have shown a significant improvement in error rates for data systems. Finally, the complete FFSR circuit is capable of single chip integration using current LSI techniques and, as such, represents a simple add-on convenience circuit to pilot tone SSB systems.

APPENDIX I

DERIVATION OF RESIDUAL MODULATION DEPTH J RESULTING FROM IMPERFECTIONS IN THE FILTER AMPLITUDE AND PHASE RESPONSE

Equation (39) gives the regenerated envelope, $r(t)$, as

$$r(t) = \frac{A_1}{B_1} \frac{(1 + R^2A^2 + 2RA \cos\{2\omega_d t + (\omega_p - \omega_d)(\tau_a + \tau_{a1}) - (\omega_p + \omega_d)(\tau_a + \tau_{a2})\})^{1/2}}{(1 + R^2B^2 + 2RB \cos\{2\omega_d t + (\omega_r - \omega_d)(\tau_b + \tau_{b1}) - (\omega_r + \omega_d)(\tau_b + \tau_{b2})\})^{1/2}}. \quad (68)$$

By making the substitutions

$$\alpha = (\omega_p - \omega_d)(\tau_a + \tau_{a1}) - (\omega_p + \omega_d)(\tau_a + \tau_{a2})$$

$$\beta = (\omega_r - \omega_d)(\tau_b + \tau_{b1}) - (\omega_r + \omega_d)(\tau_b + \tau_{b2})$$

$$G = \frac{2RA}{1 + R^2A^2}$$

$$H = \frac{2RB}{1 + R^2B^2},$$

the envelope expression of (68) can be rewritten as

$$r(t) = \frac{A_1(1 + R^2A^2)^{1/2}}{B_1(1 + R^2B^2)^{1/2}} \frac{\{1 + G\cos(2\omega_d t + \alpha)\}^{1/2}}{\{1 + H\cos(2\omega_d t + \beta)\}^{1/2}}. \quad (69)$$

To determine the residual modulation depth J, it is convenient to rewrite (69) with the substitution $x = \tan(\omega_d t)$, such that $\cos(2\omega_d t) = (1 - x^2)/(1 + x^2)$ and $\sin(2\omega_d t) = 2x/(1 + x^2)$:

$$y = \frac{r^2(t)}{k^2} = \frac{1 + G\cos\alpha\left(\frac{1 - x^2}{1 + x^2}\right) - G\sin\alpha\left(\frac{2x}{1 + x^2}\right)}{1 + H\cos\beta\left(\frac{1 - x^2}{1 + x^2}\right) - H\sin\beta\left(\frac{2x}{1 + x^2}\right)} \quad (70)$$

where

$$k = \frac{A_1(1 + R^2A^2)^{1/2}}{B_1(1 + R^2B^2)^{1/2}}.$$

Expanding (70) and solving for x gives

$$x = \frac{G\sin\alpha - yH\sin\beta \pm \sqrt{(yH\sin\beta - G\sin\alpha)^2 - (1 - y)^2 + (G\cos\alpha - yH\cos\beta)^2}}{1 - y - Hy\cos\beta + G\cos\alpha} \quad (71)$$

and since $x = \tan\omega_d t$, then

$$\omega_d t = \tan^{-1}(x). \quad (72)$$

From (71) and (72) the solution of $\omega_d t$ in terms of $f(y)$ is apparently only single valued when the square root term is zero, corresponding to the maxima or minima of the envelope term $f(y)$, denoted y_m. Equating the square root term to zero gives

$$(y_m H\sin\beta - G\sin\alpha)^2 - (1 - y_m)^2 + (G\cos\alpha - y_m H\cos\beta)^2 = 0 \quad (73)$$

such that

$$y_m = \frac{1 - GH\cos(\alpha - \beta) \pm \sqrt{G^2H^2\cos^2(\alpha - \beta) - G^2H^2 + G^2 + H^2 - 2GH\cos(\alpha - \beta)}}{1 - H^2}. \quad (74)$$

Thus the residual modulation depth J defined by (41) is given by

$$J = \frac{1 - GH\cos(\alpha-\beta) + \sqrt{G^2H^2\cos^2(\alpha-\beta) - G^2H^2 + G^2 + H^2 - 2GH\cos(\alpha-\beta)}}{1 - GH\cos(\alpha-\beta) - \sqrt{G^2H^2\cos^2(\alpha-\beta) - G^2H^2 + G^2 + H^2 - 2GH\cos(\alpha-\beta)}}. \tag{75}$$

APPENDIX II

DERIVATION OF INSTANTANEOUS FREQUENCY DEVIATION

A. Residual Output Frequency Deviation

From (40), the residual phase modulation is given by

$$v(t) = \tan^{-1}\left\{\frac{\sin(\omega_d t + \gamma_1) - RA\sin(\omega_d t + \gamma_2)}{\cos(\omega_d t + \gamma_1) + RA\cos(\omega_d t + \gamma_2)}\right\} - \tan^{-1}\left\{\frac{\sin(\omega_d t + \gamma_3) - RB\sin(\omega_d t + \gamma_4)}{\cos(\omega_d t + \gamma_3) + RB\cos(\omega_d t + \gamma_4)}\right\} \tag{76}$$

when

$$\gamma_1 = (\omega_p - \omega_d)(\tau_a + \tau_{a1})$$
$$\gamma_2 = -(\omega_p + \omega_d)(\tau_a + \tau_{a2})$$
$$\gamma_3 = (\omega_r - \omega_d)(\tau_b + \tau_{b1})$$
$$\gamma_4 = -(\omega_r + \omega_d)(\tau_b + \tau_{b2}).$$

If we now consider the first term of (76) and differentiate with respect to time, the resulting instantaneous frequency deviation is given as

$$v_1'(t) = \frac{1}{1 + \left\{\frac{\sin(\omega_d t + \gamma_1) - RA\sin(\omega_d t + \gamma_2)}{\cos(\omega_d t + \gamma_1) + RA\cos(\omega_d t + \gamma_2)}\right\}^2} \frac{d}{dt} \cdot \frac{\sin(\omega_d t + \gamma_1) - RA\sin(\omega_d t + \gamma_2)}{\cos(\omega_d t + \gamma_1) + RA\cos(\omega_d t + \gamma_2)} \tag{77}$$

so that

$$v_1'(t) = \frac{[\cos^2(\omega_d t + \gamma_1) - R^2A^2\cos^2(\omega_d t + \gamma_2) + \sin^2(\omega_d t + \gamma_1) - R^2A^2\sin^2(\omega_d t + \gamma_2)]\,\omega_d}{[\cos(\omega_d t + \gamma_1) + RA\cos(\omega_d t + \gamma_2)]^2 + [\sin(\omega_d t + \gamma_1) - RA\sin(\omega_d t + \gamma_2)]^2} \tag{78}$$

which, after simplification, gives

$$v_1'(t) = \frac{(1 - R^2A^2)\omega_d}{1 + R^2A^2 + 2RA\cos(2\omega_d t + \alpha)} \tag{79}$$

when $\alpha = \gamma_1 + \gamma_2$.

Differentiation of the second term in (76) gives a similar result such that the residual instantaneous deviation $v'(t)$ of the corrected output is given by

$$v'(t) = \frac{(1 - R^2A^2)\omega_d}{1 + R^2A^2 + RA\cos(2\omega_d t + \alpha)} - \frac{(1 - R^2B^2)\omega_d}{1 + R^2B^2 + 2RB\cos(2\omega_d t + \beta)}, \tag{80}$$

where $\beta = \gamma_3 + \gamma_4$.

B. Input Frequency Deviation

The input phase modulation resulting from multipath propagation effects is given in (27) by

$$y(t) = \tan^{-1}\left\{\frac{\sin\omega_d t - R\sin\omega_d t}{\cos\omega_d t + R\cos\omega_d t}\right\}. \tag{81}$$

The instantaneous frequency deviation from (79) is then

$$y'(t) = \frac{(1 - R^2)\omega_d}{1 + R^2 + 2R\cos 2\omega_d t} \tag{82}$$

since $A = 1$ and $\alpha = 0$.

ACKNOWLEDGMENT

The authors are grateful to Prof. T. E. Rozzi, Head of Electronics Group, for the provision of facilities to conduct this research work and to the South West Universities Computer Network for running the computer programs. Finally, they are particularly indebted to Dr. D. F. Burrows for his valuable advice and to J. R. Ball, British Telecom Research Laboratories, for providing the Rayleigh fading simulator.

REFERENCES

[1] B. B. Lusignan, "Single-sideband transmission for land mobile radio," *IEEE Spectrum*, pp. 33–37, July 1978.
[2] W. Gosling, J. P. McGeehan, and P. G. Holland, "Receivers for the Wolfson SSB/VHF land mobile radio system," *Proc. IERE Conf. Radio Receivers and Associated Systems*, July 1978, pp. 169–178.
[3] R. Wells, "SSB for VHF mobile radio at 5 kHz channel spacing," *Proc. IERE Conf. Radio Receivers and Associated Systems*, July 1978, pp. 29–36.
[4] J. P. McGeehan and D. F. Burrows, "Large signal performance of feedback automatic gain control systems," *Proc. Inst. Elec. Eng.*, Part F, vol. 128, no. 2, pp. 110–117, 1981.
[5] J. D. Parsons, M. Henze, P. A. Ratliff, and M. J. Withers, "Diversity techniques for mobile radio reception," *Radio Electron. Eng.*, vol. 45, pp. 357–367, 1975.
[6] S. W. Halpern, "The theory and operation of an equal gain pre-

detection regenerative diversity combiner with Rayleigh fading channels," *IEEE Trans. Commun.*, vol. COM-22, pp. 1099–1106, 1974.

[7] J. P. McGeehan and D. F. Burrows, "Performance limits of feedforward automatic gain control in mobile radio receivers," *Proc. Inst. Elec. Eng.*, Part F, no. 6, pp. 385–392, 1981.

[8] W. C. Jakes, Ed., *Microwave Mobile Communications*. New York: Wiley-Interscience, 1974.

[9] K. W. Leland and N. R. Sollenberger, "Impairment mechanisms for SSB mobile communications at UHF with pilot-based Doppler/fading correction," *Bell System Tech. J.*, vol. 59, pp. 1923–1942, 1980.

[10] D. F. Burrows and J. P. McGeehan, "The application of feedforward automatic gain control to mobile radio receivers as a means of reducing multipath interference," Inst. Elec. Eng. Colloq. Modern Techniques for Combatting Multipath Interference in Radio, Radar and Sonar Systems, Dig. 62/79, pp. 10.1–10.5, Nov. 1979.

[11] J. P. McGeehan, D. F. Burrows, and A. J. Bateman, "The use of 'transparent' tone-in-band (TTIB) and feedforward signal regeneration (FFSR) in single sideband mobile communications systems," in *Proc. Inst. Elec. Eng. Conf. Communications 82*, pp. 121–126, 1982.

[12] J. R. Ball and D. W. J. Holmes, "An ssb with pilot receiver for mobile radio," Clerk Maxwell Commemorative Conf. on Radio Receivers and Associated Systems, *IERE Proc. 50*, pp. 429–435, 1981.

[13] B. B. Lusignan, "The use of amplitude companded SSB in the mobile radio bands: a progress report," Communications Satellite Planning Center, Stanford University, Stanford, CA, Jan. 1980.

[14] J. P. McGeehan and A. J. Bateman, "Subjective performance of amplitude companding in SSB mobile radio systems," *Electron. Lett.*, vol. 17, pp. 859–860, Oct. 1981.

[15] J. R. Ball, "A real-time fading simulator for mobile radio," *Radio Electron. Eng.*, vol. 52, pp. 475–478, 1982.

[16] G. A. Arredondo and J. I. Smith, "Voice and data transmission in a mobile radio channel at 850 MHz," *IEEE Trans. Veh. Technol.*, vol. VT-26, pp. 88–93, 1977.

Joseph P. McGeehan was born in Bootle, Merseyside, on February 15, 1946. He received the B.Eng. and Ph.D. degrees in electrical engineering from the University of Liverpool in 1967 and 1972, respectively.

From 1970 to 1972 he held the position of Senior Scientist at the Allen Clark Research Centre, The Plessey Company Ltd., where he was primarily concerned with research into solid-state microwave devices and their applications. In September 1972, he was appointed Lecturer in the School of Electrical Engineering at the University of Bath and has led a project team conducting research into the application of signal processing techniques to single sideband mobile radio communication systems. He is the author of 40 scientific papers. In recent years, he has served as a member of the U.K. Home Office (Directorate of Radio Technology) Working Group on single sideband land mobile radio.

Dr. McGeehan is a member of U.K. Study Group 8A of CCIR.

Andrew Bateman was born in Poole, England, on September 3, 1959. He received a first class honors degree in electrical and electronic engineering from Bath University, England, in 1981.

Since 1981 he has been undertaking research into signal processing for SSB mobile radio receivers at Bath University leading to the Ph.D. degree.